Structure, Volume *32*

Supplemental Information

Structural and functional insights into tRNA recognition by human tRNA guanine transglycosylase

Katharina Sievers, Piotr Neumann, Lukas Sušac, Stefano Da Vela, Melissa Graewert, Simon Trowitzsch, Dmitri Svergun, Robert Tampé, and Ralf Ficner

Supplemental information

Structural and functional insights into tRNA recognition by human tRNA guanine transglycosylase

Katharina Sievers, Piotr Neumann, Lukas Sušac, Stefano Da Vela, Melissa Graewert, Simon Trowitzsch, Dmitri Svergun[3], Robert Tampé and Ralf Ficner

Figure S1: *Secondary structure elements of human TGT. Related to Figure 1. Secondary structure elements of human QTRT1 (left) and QTRT2 (right) are shown. Elements and residue numbers named in the main text are labelled. Blue elements form the central $(\beta\alpha)_8$ core of each domain. Insertions to the $(\beta\alpha)_8$ core are depicted in grey. Elements discussed as tRNA binding motifs in the main text are highlighted in yellow.*

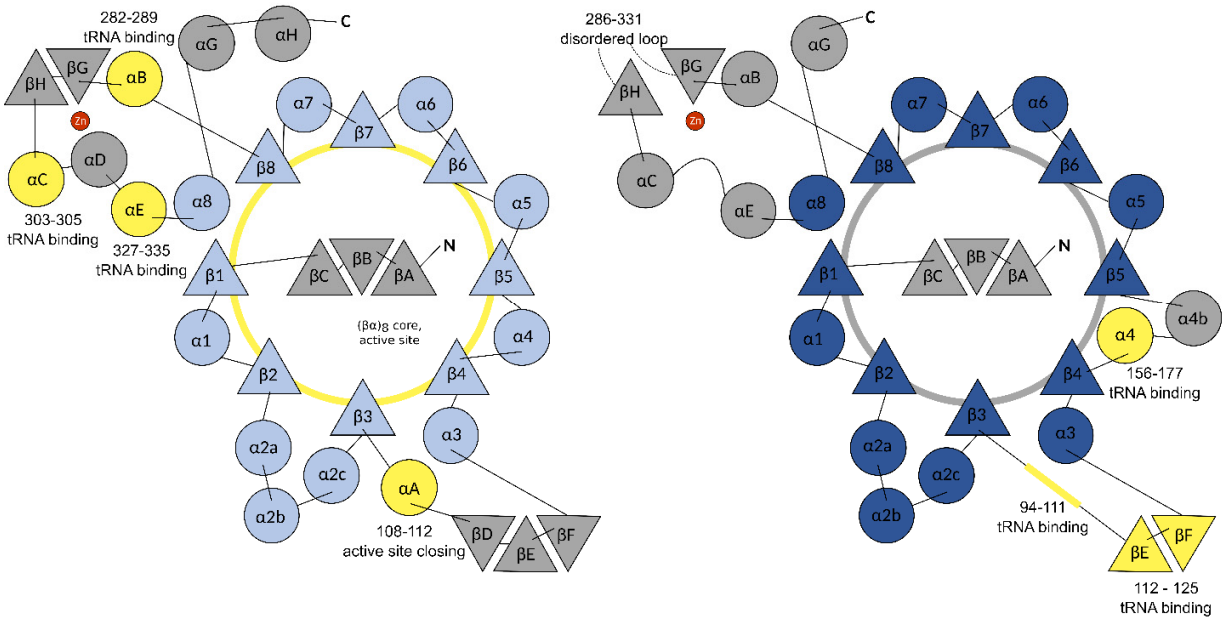

***Figure S2**: Overview of cryo-EM map quality and model fit. Rrelated to STAR methods. **a)** Cryo-EM map of the TGT·tRNA complex, colored by local resolution, on the right the cartoon representation of the atomic model color-coded by refined Atomic Displacement Factors (ADPs). **b)** Azimuth plot showing distribution of viewing orientations. **c)** Fourier-shell correlation curves of cryo-EM half maps. **d)** Particle distribution in latent space. Axes x, y, and z represent the three most important variability modes as determined by 3D Variability Analysis of the cleaned particle stack. **e)** Schematic depiction of "sweeping" tRNA motion against the TGT protein. tRNA molecule (top) is marked with arrows, TGT is visible in the background. The figure is based on 3D Variability analysis and represents the two most extreme tRNA conformations. **f)** Representative examples of map quality at different regions of the TGT·tRNA complex*

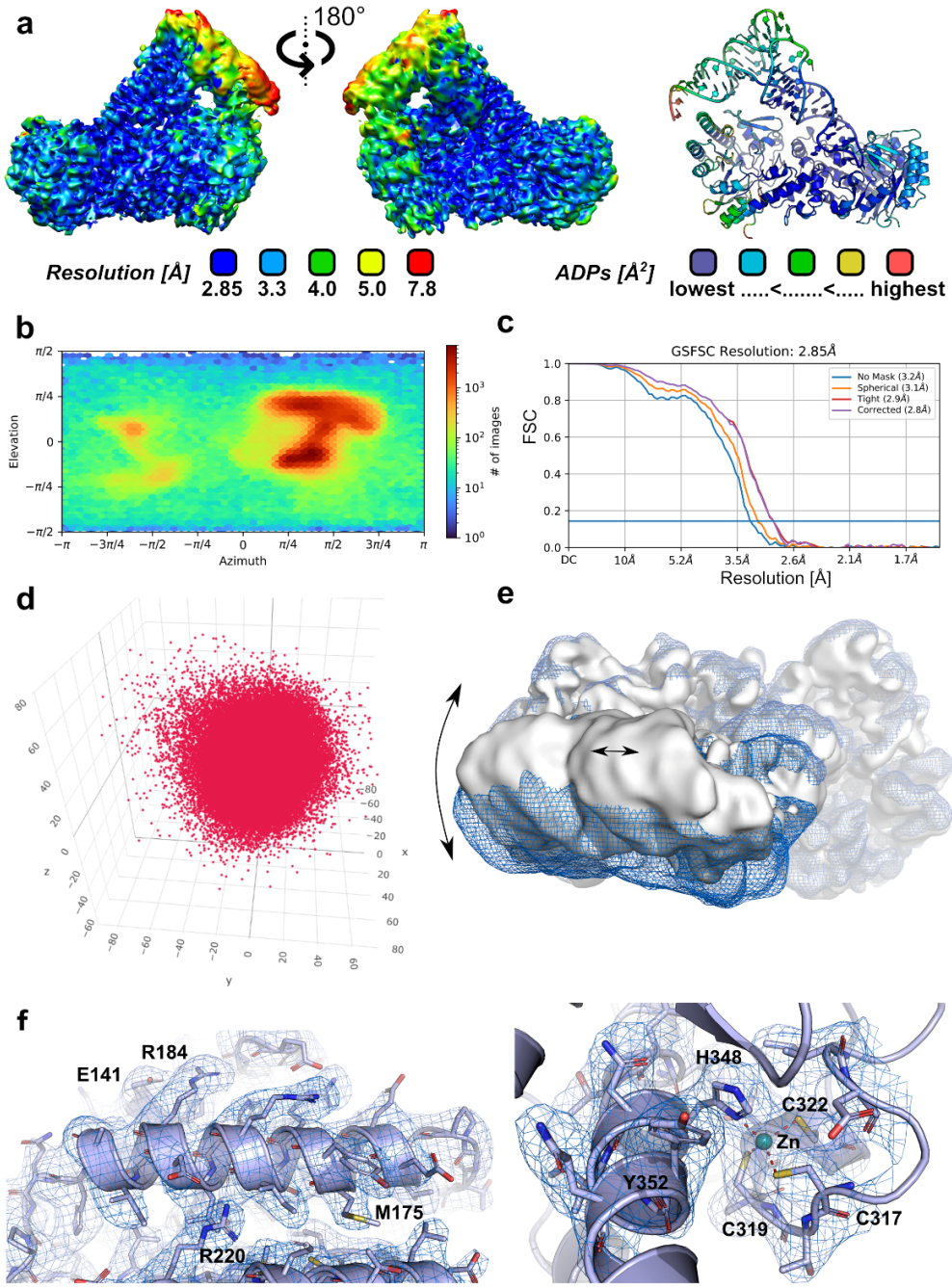

***Figure S3**: Processing of cryo-EM data. Related to STAR methods. a) Two exemplary micrographs of the dataset. b) CTF fit histogram of the dataset. c) Ab initio reconstructions and heatmap showing particle orientations d) Flow-chart summarizing data processing, details in methods. e) Representative 2D class averages. f) Comparison of the cryo-EM map quality at the active site between the homogenous and the non-uniform refinement (top). Bottom – individual cryo-EM 3D reconstructions (left: homogenous refinement, right: non-uniform refinement). The final model is depicted as a mixture of cartoon, stick and ball-and-stick representation.*

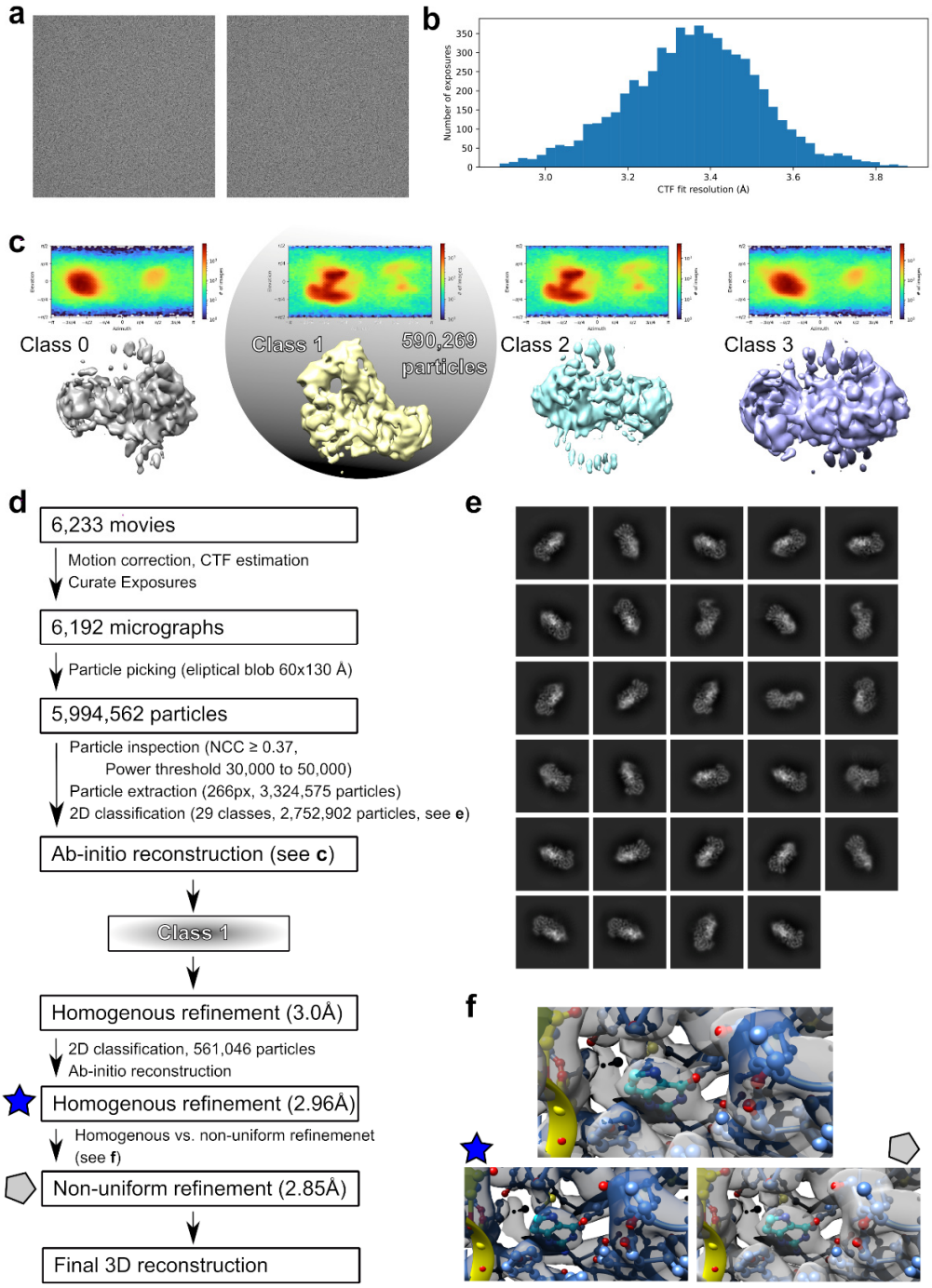

***Figure S4**: Supplementary SAXS figures. Related to Figure 2. a) SEC-SAXS profile of apo TGT showing average intensity vs frame number (blue). The Rg estimate for each frame number is shown grey and black. b) SEC-SAXS profile of TGT·tRNA complex showing average intensity vs frame number (blue). The Rg estimate for each frame number is shown in grey and black. c) SEC-RI-UV-MALLS profile of apo TGT. The molecular weight calculated from MALLS data is shown in black. d) SEC-RI-UV-MALLS profile of TGT·tRNA. The molecular weight calculated from MALLS data is shown in black. The theoretical molecular weight of the complex (116 kDa) and apo protein (90 kDa) is indicated for clarity. e) Comparison of SAXS curves of apo TGT (blue) and TGT·tRNA complex (green). f) Comparison of pair-distance distribution functions calculated for apo TGT (blue) and TGT·tRNA complex (green) SAXS data. g) Experimental SAXS data for apo TGT with fit of calculated pair-distance-distribution function. h) Experimental SAXS data for TGT·tRNA complex with fit of calculated pair-distance-distribution function.*

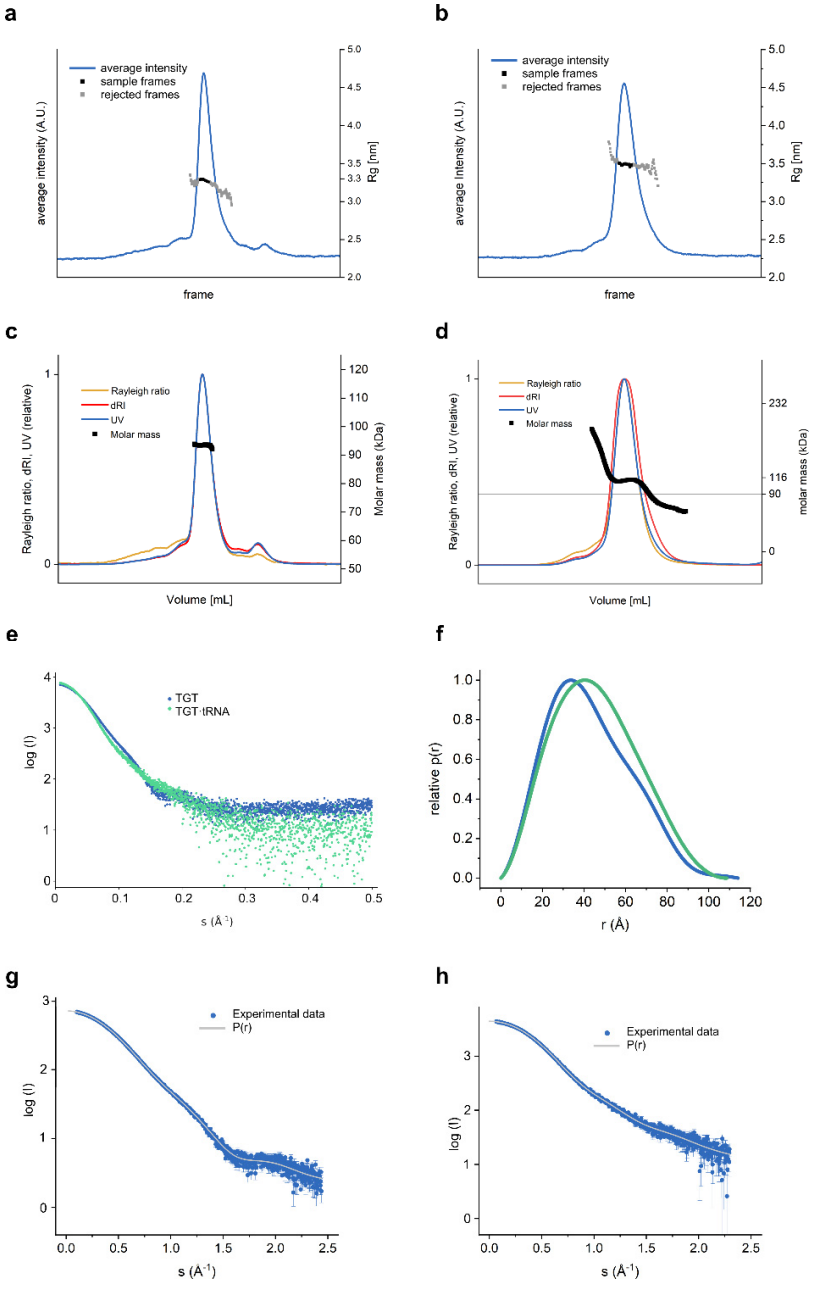

***Figure S5**: Ensemble optimization with structure pool based on TGT cryo-EM or crystal structure. Related to Figure 3. a) Dimensionless Kratky-plot of TGT SAXS data, with theoretical scattering of an optimized ensemble that was selected from structures based on a TGT crystal structure (PDB: 7NQ4). The fit against the experimental data is expressed as χ^2. The crosshair marks $sR_g = \sqrt{3}$ and $(sR_g)^2 \times I(s)/I(0) = 3e^{-1}$. b) Distribution of the radii of gyration (R_g) of structures in pool and the optimized ensemble. c) Structures in the ensemble. Domains modelled as a rigid body are shown in grey, disordered regions modelled as random chains are shown in yellow.*

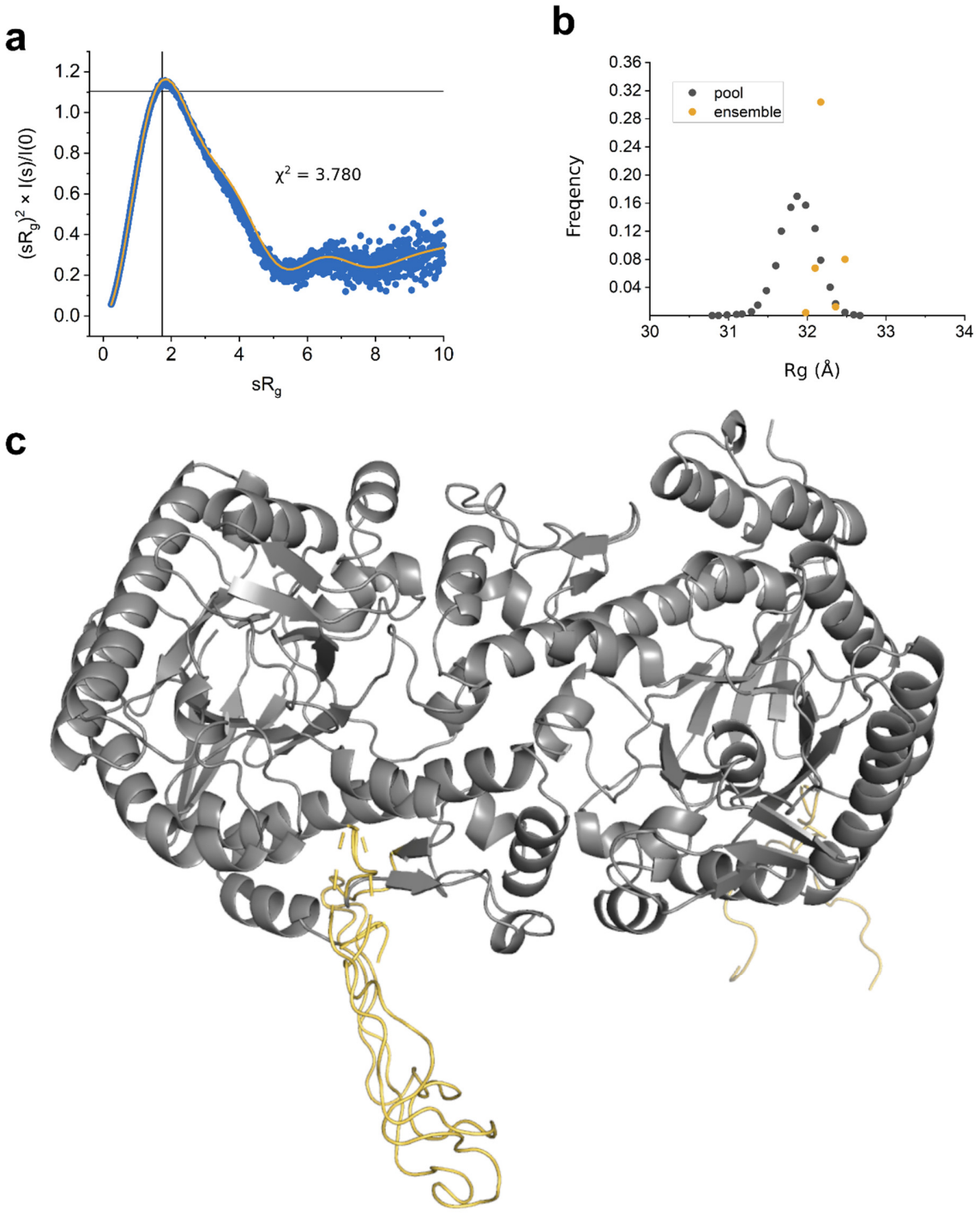

***Figure S6**: Raw fluorescence polarization data and curve fits. Related to Figure 4. a-b) Fluorescence polarization data obtained for varying concentrations of TGT R159E (a) or TGT K162E (b) and fluorescently labelled $tRNA^{Asp}$. c-f) Fluorescence polarization data obtained for varying concentrations of TGT and four fluorescently labelled RNA constructs: c) $tRNA^{Asp}$, d) $tRNA^{Asp}$ ASL, e) $tRNA^{Tyr}$ ASL and f) A20 RNA. For b-f), the average and standard deviation of three replicates as well as the fitted curve (red) is shown. For a), the average and standard deviation of two replicates is shown. Error bars in panel f are smaller than the symbol. Data is not* normalized.

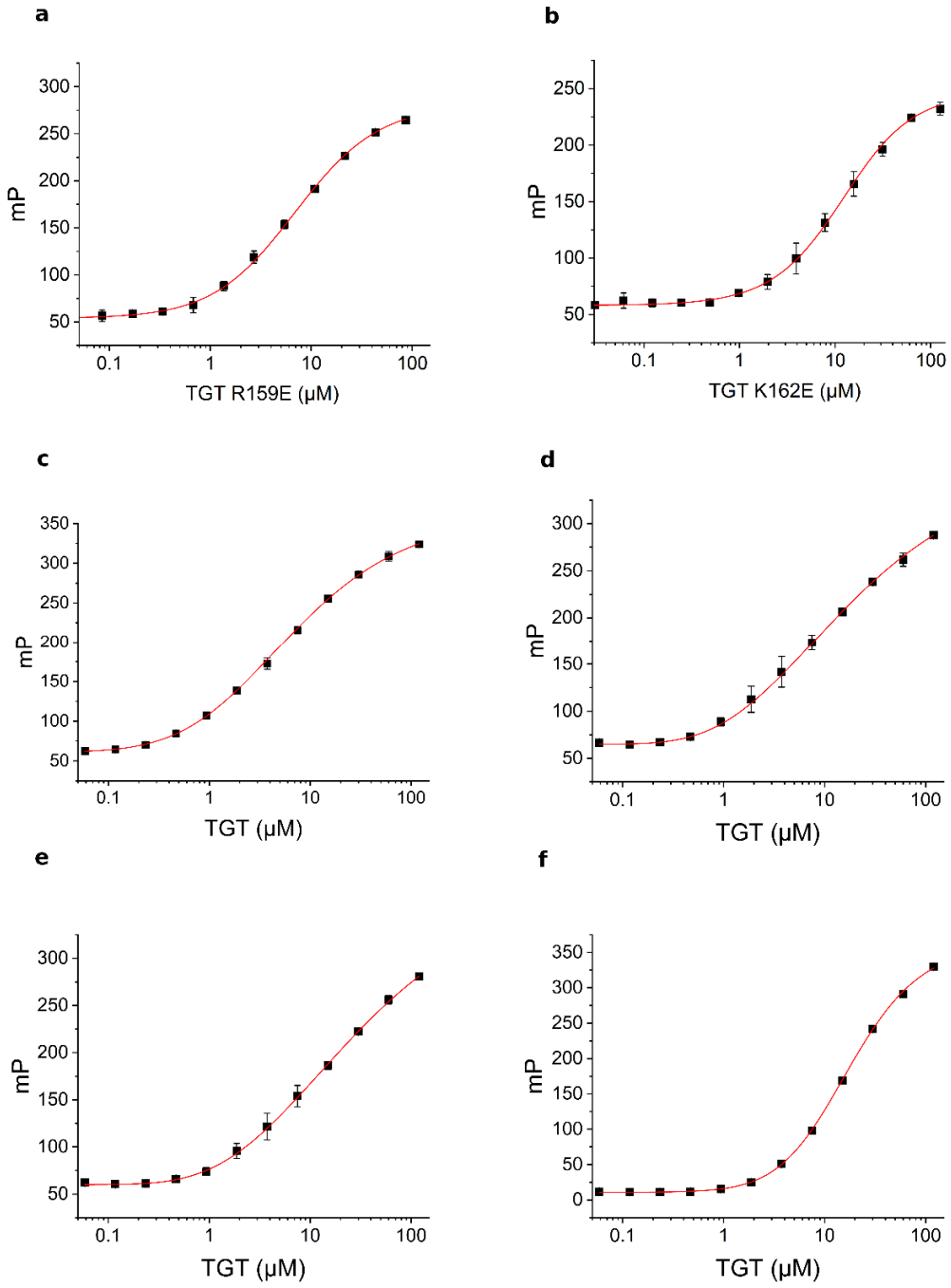

***Figure S7**: Gel images used for Q-incorporation activity test. Related to Figure 6. Each gel image shows the separated samples taken from a Q-incorporation reaction (contrast linearly increased). Lanes 1-7 correspond to samples taken after 2, 3, 5, 10, 20 and 30 minutes. Lower bands are comprised of unmodified RNA, upper bands represent Q-modified RNA. Q-incorporation reactions were carried out with varying RNA substrate concentrations: a) 17.7 µM $tRNA^{Asp}$ ASL b) 8.8 µM $tRNA^{Asp}$ ASL c) 5.9 µM $tRNA^{Asp}$ ASL d) 3.5 µM $tRNA^{Asp}$ ASL e) 1.8 µM $tRNA^{Asp}$ ASL f) 0.9 µM $tRNA^{Asp}$ ASL g) 14.0 µM $tRNA^{Asp}$ h) 7.0 µM $tRNA^{Asp}$ i) 4.7 µM $tRNA^{Asp}$ j) 2.8 µM $tRNA^{Asp}$ k) 1.4 µM $tRNA^{Asp}$ l) 0.7 µM $tRNA^{Asp}$.*

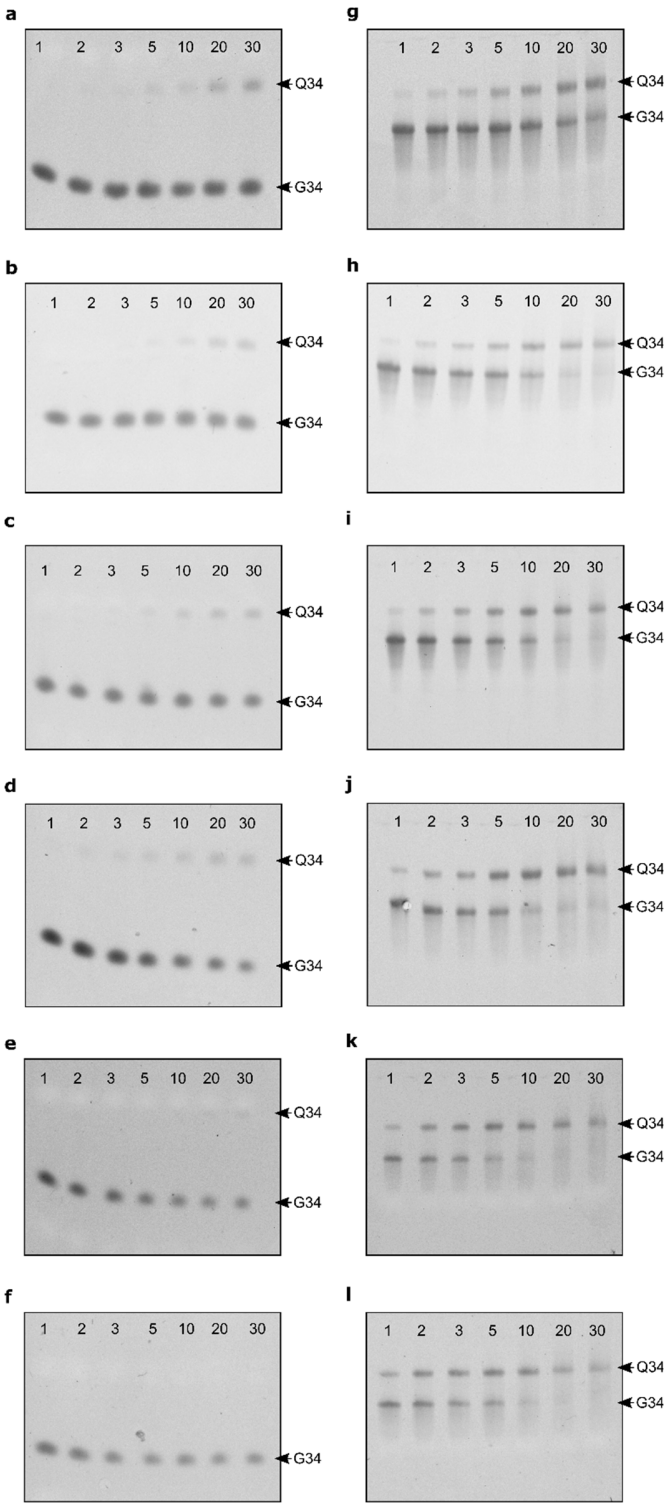

Supplemental tables

Supplementary table 1: Cryo electron microscopy data collection, data processing and refinement statistics. Related to STAR methods.

Data collection and processing	**TGT·tRNA complex**
Microscope	Thermo Scientific Glacios
Magnification (×)	190,000
Voltage (kV)	200
Dose rate (e^- pixel^{-1} s^{-1})	0.78
Total electron exposure (e^- Å^{-2})	42
Defocus range (μm)	−1.0 to –2.0
Camera	Falcon 3EC direct electron detector
Pixel size (Å)	0.78
Number of frames per movie	38
Number of movies	6,192
Data processing software	CryoSPARC[67]
Initial particle images	5,994,562
Final particle images	561,046
Map resolution (Å)	2.85
FSC threshold	0.143
Map resolution range (Å)	1.67-36.37
Map sharpening B factor (Å^2)	0
Refinement	
Initial models used (PDB codes)	7NQ4, 2TRA
Model composition	
Non-hydrogen atoms	7626
Residues (protein)	772
Residues (RNA)	75
Model to map fit	
CCmask	0.8712
CCvolume	0.8576
CCpeaks	0.8018
R.m.s. deviations	
Bond lengths (Å)	0.009
Bond angles (°)	0.963
Ramachandran plot	
Favored (%)	91.9
Allowed (%)	8.1
Disallowed (%)	0
Validation	
All-atom clashscore	6.15

Rotamer outliers (%)	6.3
Accession codes	
EMDB	EMD-16976
PDB	8OMR

Supplementary table 2: Details of SAXS data collection and primary data analysis. Related to STAR methods.

Sample details	**TGT**	**TGT·tRNA complex**
Scattering particle composition	QTRT1, QTRT2	QTRT1, QTRT2, GGG-*hs*tRNA
Buffer composition	20 mM HEPES pH 7.5, 100 mM NaCl, 3 % (w/v) glycerol	
Temperature (°C)	4 ˚C (storage), 20 ˚C (measurement)	
Size Exclusion Chromatography (SEC-SAXS)		
Sample injection concentration (µg/µL)	10.0	4.5
Sample injection volume (µL)	75	75
SEC column type	S200 300/10 increase	
SEC flowrate (mL/min)	0.5	0.7
Online MALS-RI		
Molecular mass, theoretical (kDa)	90.9	116.3
Molecular mass, MALS-RI (kDa)	93 ± 5	111.8 ± 1.3
SAXS data collection		
In-beam sample cell	1-mm quartz capillary	
Radiation source	Synchrotron (Petra III, beamline P12, EMBL Hamburg)[76]	
Wavelength (Å)	1.23980	
Detector	Pilatus 6M	
Measured s-range ($Å^{-1}$)	2.23×10^{-3} - 7.31×10^{-1}	2.43×10^{-3} - 7.37×10^{-1}
Data acquisition/reduction software	SASFLOW[77]	
Exposure time/frame (s)	0.995000	
Number of frames	3600	2160
Sample frames used for averaging	34	38
Solvent blank	Column flow-through	
SAXS-derived structural parameters		
Methods/Software	PRIMUS, GNOM[73]	
Guinier Analysis		
R_g ± σ (Å)	32.8 ± 0.0	34.8 ± 0.0
min < sR_g < *max* limit	0.33 - 1.27	0.23 - 1.27
Linear fit assessment (Fidelity)	0.41	0.34
PDDF/P(r) analysis		
R_g (Å)	33.2	35.2
R_{max} (Å)	114	109
s-range ($Å^{-1}$)	$1.00 \times 10^{-3} – 2.44 \times 10^{-1}$	$0.66 \times 10^{-3} – 2.29 \times 10^{-1}$
Volume estimates		
Porod volume ($Å^3$)	125095	159665

Molecular weight estimates		
Bayesian Inference Credibility Interval (kDa), (probability)	67.9 - 90.0, (92.98)	92.7 - 106.9, (90.49)

Modelling

Methods/Software	Ensemble optimization method (RANCH, GAJOE)[74]	
s-range for fit ($Å^{-1}$)	$7.25 \times 10^{-3} – 5.00 \times 10^{-1}$	$7.14 \times 10^{-3} – 5.00 \times 10^{-1}$
Ensemble name	Cryo-EM structure-based	Cryo-EM structure-based
Atomic structure (PDB-ID)	8OMR	8OMR[a]
Residues	QTRT1 16-405, QTRT2 1-292, 329-414	QTRT1 16-405, QTRT2 1-292, 329-414, tRNA 1-78
Loop modelling	random	random
Residues	QTRT1 (-2)-15, , QTRT2 293-328, QTRT2 415	QTRT1 (-2)-15, QTRT2 293-328, QTRT2 415
Number of models in ensemble	2	3
χ^2	1.300	1.662
Ensemble name	Crystal structure-based	
Atomic structure (PDB-ID)	7NQ4	
Residues	QTRT1 16-405, QTRT2 1-292, 326-414	
Loop modelling	random	
Residues	QTRT1 (-2)-15, , QTRT2 293-325, QTRT2 415	
Number of models in ensemble	2	
χ^2	3.780	

Accession codes

SASDB	SASDRB8	SASDRC8

[a] sequence adjusted and 5’ GGG residues modeled using Rosetta FARFAR2[78,79]